Evidence of non collisional femtosecond laser energy deposition in dielectric materials

G Duchateau, B Chimier, S Coudert, E Smetanina, L Barilleau, N Fedorov, H Jouin, G Geoffroy, Patrick Martin, V T Tikhonchuk

▶ **To cite this version:**

G Duchateau, B Chimier, S Coudert, E Smetanina, L Barilleau, et al.. Evidence of non collisional femtosecond laser energy deposition in dielectric materials. Physical Review B: Condensed Matter (1978-1997), 2020. hal-03023632

HAL Id: hal-03023632
https://hal.science/hal-03023632

Submitted on 25 Nov 2020

HAL is a multi-disciplinary open access archive for the deposit and dissemination of scientific research documents, whether they are published or not. The documents may come from teaching and research institutions in France or abroad, or from public or private research centers.

L'archive ouverte pluridisciplinaire **HAL**, est destinée au dépôt et à la diffusion de documents scientifiques de niveau recherche, publiés ou non, émanant des établissements d'enseignement et de recherche français ou étrangers, des laboratoires publics ou privés.

Evidence of non collisional femtosecond laser energy deposition in dielectric materials

G. Duchateau*, B. Chimier, S. Coudert, E. Smetanina, L. Barilleau,
N. Fedorov, H. Jouin, G. Geoffroy, P. Martin, and V.T. Tikhonchuk
Université de Bordeaux-CNRS-CEA, Centre Lasers Intenses et Applications,
*UMR 5107, 351 Cours de la Libération, 33405 Talence, France**
(Dated: November 25, 2020)

Electron dynamics in the bulk of large band gap dielectric crystals induced by intense femtosecond laser pulses at 800 nm is studied. With laser intensities (a few 10 TW/cm^2) under the ablation threshold, electrons with unexpected energies in excess of 40-50 eV are observed by using the photoemission spectroscopy. A theoretical approach based on the Boltzmann kinetic equation including state-of-the-art modeling for various particles interactions is developed to interpret these experimental observations. A direct comparison shows that both electron heating in the bulk and a further laser field acceleration after ejection from the material contribute equivalently to the final electron energy gain. The laser energy deposition in the material is shown to be significantly driven by a non-collisional process, i.e. direct multiphoton transitions between sub-bands of the conduction band. This work also sheds light on the contribution of the standard electron excitation/relaxation collisional processes, providing a new baseline to study the electron dynamics in dielectric materials and associated applications as laser material micromachining. To support such applications, a simple expression to evaluate the energy deposition by non collisional absorption is provided.

I. INTRODUCTION

Developments of laser facilities delivering ultrashort and intense laser pulses with photon energy in the eV range have motivated studies in laser-solid interactions including metals [1, 2], semiconductors [3] and dielectrics [4, 5]. Focusing of a femtosecond laser pulse in a transparent dielectric material may induce modifications beneath the surface, which can be tailored to produce permanent three dimensional localized structural changes [6–10]. Micromachining efficiency depends on the amount of laser energy deposited in the irradiated volume. A control of the amount and spatial shape of the deposited laser energy opens the way to a large variety of applications going from photonics, bulk microelectronics, nanofluidics, to medicine [11]. Together with advanced experimental setups, such a control can be achieved by an in-depth modeling description of the physical processes at play, i.e. laser driven electron dynamics leading to the energy deposition into the material. An accurate prediction of the laser energy deposition may further support the development of these applications and improve the knowledge of the fundamental laws governing the laser-solid interaction. So there is a strong need to accurately describe the electron dynamics in dielectric materials irradiated by femtosecond laser pulses with intensities ranging from a few TW/cm^2 to the ablation threshold.

The admitted picture for the laser energy deposition into the dielectric material is as follows. The laser energy is first absorbed by electrons through the processes of both ionization and excitation/relaxation in the conduction band. During the second stage, the absorbed laser energy is redistributed between the excited carriers which may reach higher energies while they undergo collisions with phonons, ions, and other electrons in the presence of the laser field. These processes eventually lead to the energy transfer to the lattice. This is a collisional picture theoretically described either by the Drude model, multiple rate equations [12], or the kinetic Boltzmann equation [4, 5, 13] which can provide the energy distribution of excited electrons related to the laser energy deposition. This distribution can be experimentally obtained through photoemission spectroscopy [14–17]. For laser intensities below the breakdown threshold of various dielectric materials including CsI, diamond, CeF_3, sapphire, and SiO_2, photo-emitted electrons exhibit universal characteristics of energies in excess of tens of eV which collisional heating is not able to account for [17, 18]. Following studies on High-order Harmonics Generation (HHG) in solids where such electron energies are reached [19–23], it has been suggested that the previous photoemission observations may be explained by direct multiphoton transitions between sub-bands of the conduction band, hereafter referred to as the interband process [15, 16]. A question then arises on the importance of the interband process relative to collision-assisted electron transitions, and on its contribution to the laser energy deposition in dielectric materials (which is related to the electron energy distribution).

More generally, when a dielectric material is irradiated by a femtosecond laser pulse, two main classes of processes related to the electron dynamics are generally considered independently: material modifications induced by laser energy deposition [7] and HHG [19, 20], corresponding to irreversible and reversible electron dynamics, respectively. In both cases, valence electrons are first promoted to excited states of the conduction band, the subsequent dynamics then departing between these two processes. HHG is a non collisional process related to direct electron intra- and interband transitions. The coherence between the excited electrons with the laser

* guillaume.duchateau@u-bordeaux.fr

electric field stands during at least the period of time of one optical cycle, eventually leading to the recombination of the excited electron to its parent ion (resulting in radiation emission). During the electron excursion in the conduction band, electrons may reach energies of tens of eV but only on a short period of time (this is a reversible process of energy exchange between electrons and fields). Another quantum pathway corresponds to the excitation of valence electrons to the bottom of the conduction band where they may undergo collisions (scattering with momentum exchange) with phonons or other electrons [24], then breaking their coherence with the laser electric field. This scattered electrons then may further undergo collisions, eventually leading to the laser energy deposition into the material (phonon density is increased through collisions). The occurrence of these two important processes depends on laser and material parameters.

Two main classes of models are candidate to address this question on the importance of the interband process relative to collision-assisted electron transitions leading to the laser energy deposition in dielectric materials. (i) Collisional models as solving the state-of-the-art quantum Boltzmann equation, including all possible electronic excitation and relaxation processes, provide the electron energy distribution [4, 5, 12]. But the interband process has never been included except in [13]. (ii) Non collisional models based on a resolution of the time-dependent Schrödinger equation or optical Bloch equations [20–23, 25]. The former allows one to interpret the photoemission observation but the collisions are not included [15, 16]. Despite these studies, a *direct* comparison between theoretical and experimental electron energy distributions has never been performed while this is an indispensable step for validating any model [4, 5, 12, 15], leaving serious interrogations regarding the (non-equilibrium) electron dynamics in the conduction band of dielectric materials.

In the present work, the electron dynamics is studied both experimentally and theoretically for α-quartz (cristalline SiO_2) which is a representative example of large band gap dielectrics. The experimental setup and the observed photoelectron energy distributions for various laser intensities are presented in Section II. The theoretical model providing a kinetic description of the laser induced electron dynamics both inside the bulk and after ejection is provided in Section III. It is based on a resolution of the quantum Boltzmann equation including all possible bulk excitation/relaxation processes coupled to a subsequent laser driven field acceleration (LDFA) of electrons after their ejection [26]. In Section sec:results, the observed photoelectron energy distributions are *directly* comparedwith the theoretical predictions, within the challenging accuracy-demanding linear scale in the present context. We emphasize that only the maximum energy of ejected electrons has been considered in previous works [13, 17, 18]. The present model allows to predict photoelectron spectra which are in a good agreement with experimental results for various laser intensities. The non collisional direct multiphoton transitions between sub-bands of the conduction band make a significant heating of electrons in dielectric materials in contrast to the widely used assumption of a dominant role of collisional processes including phonon-assisted photon absorption and inverse Bremsstrahlung. Our model accounts in particular for acceleration of electrons to energies in excess of 40 eV below the ablation threshold. For application purpose as laser micromachining of materials, a simple expression to evaluate the energy deposition by non collisional absorption is provided. Finally conclusions of this work are drawn in Section V.

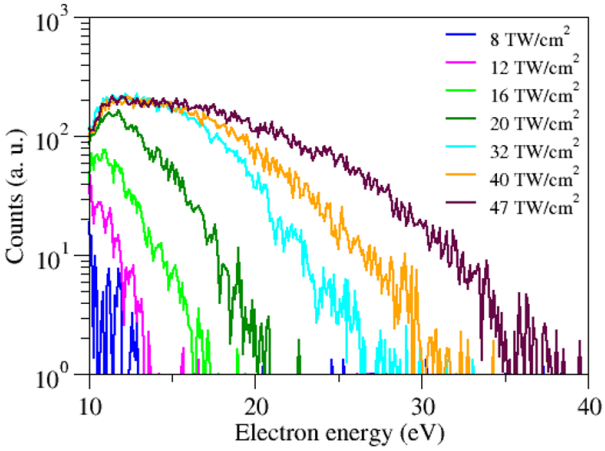

FIG. 1. Experimental photoelectron energy distribution for quartz. Only the region of highest electron energies is shown, where dynamics is only due to intrinsic processes modeled in the present study (see text for more details).

II. EXPERIMENTAL OBSERVATIONS

The experiment is carried out on the CELIA Aurore Ti:saphire laser facility [27]. A 1 mm thick α-quartz target is irradiated by linearly P-polarized pulses at the wavelength of $\lambda = 800$ nm, with 70 fs duration (full width at half maximum, FWHM) at 1 kHz repetition rate. The incident angle is 45° and a 30 mm lens produced a Gaussian intensity distribution in a 21 µm spot size (FWHM). The experiment is conducted in a vacuum chamber at a pressure of 10^{-9} Torr, and the sample is heated homogeneously to a temperature of 800 K to maximize the photoemission yield, by decreasing the surface charge. The photoelectrons emitted from the surface are collected by a hemispherical analyser (CLAM IV VG Microtech) with 9 channeltrons operating in ultraviolet photo-electron spectroscopy mode. The axis of the detector is perpendicular to the sample surface.

Figure 1 shows the experimental photo-emission spectra for quartz obtained with intensities ranging from 8 to 47 TW/cm^2. In general, such spectra exhibit a main peak, for an electron energy of a few eV, which almost does not evolve with respect to the intensity. This peak

corresponds to secondary electrons which properties depend on the surface state. Since we are interested in intrinsic processes corresponding to high enough energies, the low energy region is not shown. Above roughly 11 eV, the signal exhibits a smooth decrease up to a maximal energy, E_{max}, for which at least one count is measured. E_{max} increases with respect to the intensity and reaches roughly 40 eV for the highest intensity. Note that after each photoemission experiment, we have checked by using a microscope that there was no modification of the target surface, as observed in [28]. Similar behaviors in terms of high energies and distribution shape have been obtained for other large bandgap materials as sapphire, CsI, diamond, and CeF_3 [17, 18].

III. KINETIC MODELING OF THE LASER INDUCED ELECTRON DYNAMICS

The electron dynamics in the bulk is described by a Boltzmann kinetic equation which domain of validity is fulfilled by using moderate laser intensities producing electron densities of the order of 10^{18}-10^{20} cm^{-3} [5, 12, 13]. This particle density is small enough to ensure only binary collisions and an average distance between particles larger than the De Broglie length allowing one to consider particles as evolving classically (Boltzmann equation is classical whereas collision operator are evaluated through quantum calculations). On the other hand, such densities are large enough to ensure a sufficiently large number of collisions. Depending on the collisional process, the collision frequency is in between 10^{14} s^{-1} and 10^{15} s^{-1}. Since the laser pulse duration is 70 fs, at least several collisions in average for each process take place during the interaction. The use of a distribution function thus makes sense and each collisional process is expected to have a particular influence on the shape of the distribution function.

Electrons are ejected from a nanometer-size layer beneath the target surface where the laser electric field can be considered as a constant. Indeed, the field amplitude adapts to the dielectric material property on a length-scale v_b/ω_{ve} where v_b is the velocity of bound valence electrons and ω_{ve} is their plasma frequency. The order of magnitude of these quantities is $3.\times 10^6$ m.s^{-1} and 10^{16} s^{-1}, respectively, leading to $v_b/\omega_{ve} \simeq 3$ Å. The laser intensity is thus relatively constant a few nanometers beneath the surface, implying no spatial dependence in the electron distribution, $f(\vec{k},t)$, where $\vec{k}$ is the momentum and the electron energy is $E_k = \hbar^2\vec{k}^2/2m_e$. The temporal evolution of f in the bulk is then given by:

$$\frac{\partial}{\partial t}f(\vec{k},t) = \left.\frac{\partial f(\vec{k},t)}{\partial t}\right|_{\text{ioniz}} + \left.\frac{\partial f(\vec{k},t)}{\partial t}\right|_{\text{relax}} + \left.\frac{\partial f(\vec{k},t)}{\partial t}\right|_{\text{heat}}, \quad (1)$$

where the three collision integrals in the right hand side describe the ionization, the relaxation, and the laser excitation of conduction electrons, respectively. The electron distribution is assumed to be isotropic since it is due to electron collisions with acoustic phonons which characteristic timescale is 10 fs [29].

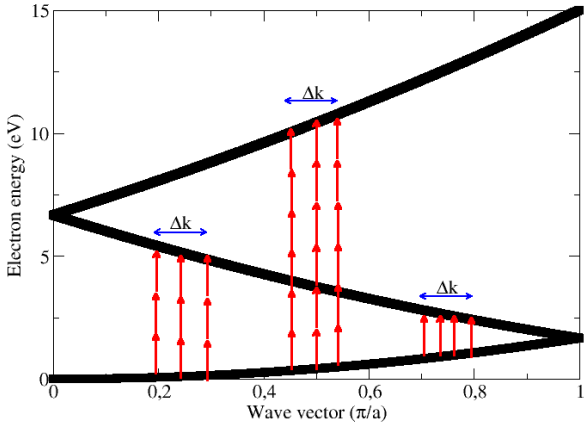

FIG. 2. Illustration of the structure of the conduction band in the first Brillouin zone as described in the multiple parabolic band model. The bands exhibit an energy bandwidth of $h\nu_c$ of the order of 1 eV due to the collisional broadening. An illustration of possible multiphoton transitions is depicted by the red arrows. Due to the broadening, the transitions take place over a wave vector region Δk.

The ionization processes consist of both the photoionization, which is evaluated through the complete Keldysh expression [30], and the impact ionization described as in [4]. The relaxation processes are related to electron-electron (e-e) [4] and electron-phonon (e-ph) [4, 29] collisions, which induce the energy exchange of electrons between themselves and to the lattice, respectively. These collision integrals are calculated with the Fermi's golden rule. The electron recombination is also included with a characteristic time of 150 fs [31] which is assumed not to depend on E_k. The energy distribution of phonons is assumed not to evolve during this short interaction time and is set to the equilibrium Bose-Einstein distribution with a lattice temperature set to 800 K.

Two main processes are included for the laser-induced excitation of conduction electrons. First, the electrons can absorb or emit simultaneously several photons during a collision with phonons (e-ph-pt) or ions (e-ion-pt, inverse Bremsstrahlung) [4]. Second, electron excitation can also take place through a non-collisional process (no other particle as ion or phonon is involved to absorb photons) which is direct multiphoton interband transitions [13, 15, 17, 18, 32]. To include the latter process, the conduction band is described by multiple parabolic energy sub-bands. An illustration of this process is provided by Fig. 2. Note this mechanism departs from the Rethfeld's approach [4, 12] and is expected to have a significant impact on the electron dynamics. The interband rate is evaluated according to the expression and parameters provided in [13], i.e. without using any fitting procedure. Such an approach allows us to introduce

explicitly the collisionless heating in a full kinetic treatment of the electron dynamics in laser-driven dielectrics [13].

Note that the photoionization process and the laser induced electron dynamics in the conduction band are described separately within the present approach whereas it may be treated on the same foot by solving optical Bloch equations for instance [20–23, 25]. Both processes are introduced separately because (i) they are of different nature and (ii) they cannot be modeled within the Boltzmann framework on the same foot. (i) They are of different nature in the sense that the multiphoton ionization process bridges a bound valence state to a quasi-free continuum state, whereas the multiphoton excitation in the conduction band bridges two continuum states. Despite the starting point of the theory to evaluate these collision rates is similar, the dipolar matrix elements are different, justifying to introduce both terms in the Boltzmann equation. (ii) The photoionization process generates electrons in the conduction band, whereas the multiphoton excitation process in the conduction band leaves the total conduction electron density unchanged. The latter process only changes the electron energy distribution in the conduction band. Within our Boltzmann model, only one parabolic conduction band is considered so that the photoionization process corresponds to a source term of electrons into the bottom of the conduction band. An additional Boltzmann equation for the valence band may be added for the sake of generality and treating on the same foot both multiphoton processes, but it influence is expected to be negligible since no more than a few percents of valence electrons are promoted to the conduction band. This approach is explained in details in [13].

Solution to the Boltzmann equation (1) provides the energy distribution of electrons in the material. Their ejection from the surface is possible if their energy is larger than the work function which is 0.9 eV for quartz [33, 34]. For low energy ejection, surface effects may modify the distribution [35]. However, this influence is negligible for the most energetic electrons which are considered here. Consequently, the distribution of ejected electrons near the surface is assumed to be the same as the one calculated in the bulk. To obtain a distribution *directly* comparable to the experimental data, $f(E_k, t)$ is first weighted by the density of states $g(E_k) \propto \sqrt{E_k}$ accounting for a three-dimensional free electron gas. Secondly, the influence of the laser electric field $F(t)$, which may further accelerate or decelerate the ejected electrons depending on their instant of emission, is taken into account: it is a laser-driven field acceleration (LDFA) which can change the energy distribution [26]. The final energy of the ejected electron is obtained by integrating the classical equation of the electron motion in vacuum $dv/dt = -eF(t)/m_e$ from the ejection moment t_e to the end of the laser pulse (160 fs in practice). The initial ejection velocity v_0 at t_e is evaluated from the calculated electron distribution in the bulk. Since electrons in the bulk undergo numerous collisions before ejection, they lose any coherence [24] with the laser electric field at the time of ejection. Consequently, the electrons are assumed to be ejected uniformly during the interaction: their ejection time is not related to any particular phase of the laser electric field. Since in experiments ejected electrons are collected over the whole laser pulse duration, the theoretical predictions are obtained by integrating the electron distribution over time. Note that the maximum energy gain corresponds to the classical energy of *half* an optical cycle. For an electron ejected at the optimal time, a simple calculation shows that the final energy is roughly 40 eV for an ejection energy $E_{k_0} = 20$ eV and a laser intensity $I = 50$ TW/cm^2.

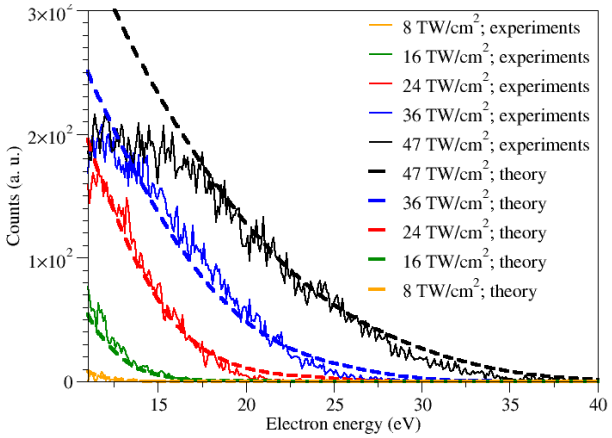

FIG. 3. Energy distributions of ejected electrons from photoemission experiments (solid lines) and modeling (dashed lines) for various laser intensities.

IV. EVIDENCE OF NON COLLISIONAL LASER ENERGY DEPOSITION

Figure 3 shows, within a linear scale, the experimental distributions of ejected electrons together with the theoretical predictions for intensities ranging from 8 to 47 TW/cm^2. The theoretical distribution at $I = 24$ TW/cm^2 is multiplied by a renormalization factor to compare to the experimental data. The same factor is used for all intensities. Both experimental and theoretical data are in a good agreement for each intensity. The only significant discrepancy between modeling and experimental spectra appears for electron energies below 17 eV for the largest laser intensity. It may be attributed to electron transport in the bulk which is not included in the present modeling: low energy electrons are sensitive to spatial charge rearrangements (potential minimization) in the bulk which are all the more important that the produced charge density is large (or highest laser intensities).

The experimental observations can be reproduced only if we include all above-mentioned physical processes: photo-ionization, impact ionization, heating through

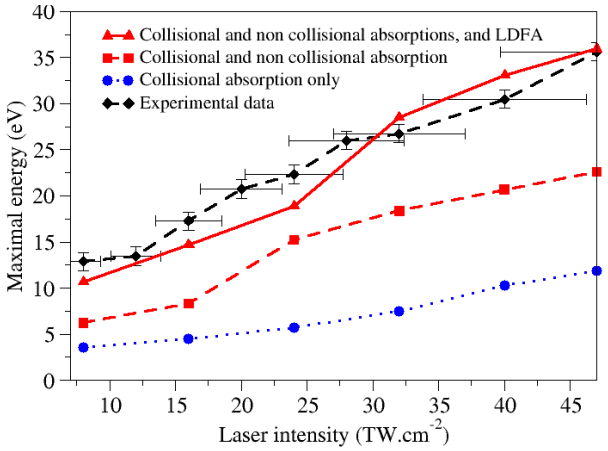

FIG. 4. Maximum energy of photoemitted electrons as a function of the laser intensity. Absorption processes are gradually switched on within the modeling, see inset legend for curves meaning.

electron-phonon-photon and interband transitions, the relaxation through electron-phonon and electron-electron collisions, and the LDFA. In order to evaluate the role of each process on the electron dynamics in the bulk, they have been successively switched off. The comparison of the theoretical spectra obtained with the various modeling configurations (not shown here) to the experimental data leads to the following conclusions. (i) the impact ionization prevents electrons from reaching too high energies at the largest intensities. However there is no electron avalanche, which is consistent with the fact that the irradiated material is not damaged. (ii) Regarding the electron heating in the conduction band, the introduction of both e-ph-pt and interband processes is required to recover correct slopes for all considered intensities. In particular, the interband process enables to mimic the smooth decrease with respect to the electron energy [13]. (iii) Regarding the relaxation, the electron-electron collisions provide a smooth energy distribution. Otherwise the electron distribution contains several peaks separated by the photon energy [13] that is not experimentally observed. The contribution of e-ph collisions also permits to redistribute electrons to lower energies providing the observed slopes. In contrast, the electron recombination and e-ion-pt do not modify significantly the spectra due to the short interaction time and relatively low ionization degree (the electron density in the conduction band is in between 10^{19} and 10^{20} cm^{-3} depending on the intensity), respectively.

Figure 4 provides the evolution of E_{max} as a function of the laser intensity from experimental observations and as predicted by the modeling (the interband and LDFA processes are included or not). In the experiment, E_{max} increases monotonically from 11 eV to roughly 40 eV. Without the interband and LDFA processes, E_{max} cannot exceed 10 eV for the highest intensity, the heating being only due to e-ph-pt collisions in that case. By including the interband process, E_{max} reaches about 23 eV, i.e. twice the energy of the previous configuration. Both e-ph-pt and interband contributions to the electron heating are thus comparable. A good agreement with the experimental data is obtained when the LDFA is included, providing an enhancement of the final electron energy of more than a factor of 2. These considerations clearly show that the observed photo-emission spectra result from three physical processes with comparable contributions. All the previous conclusions are expected to be similar for the above-mentioned other large band gap dielectric materials which exhibit similar band structures and coupling between states.

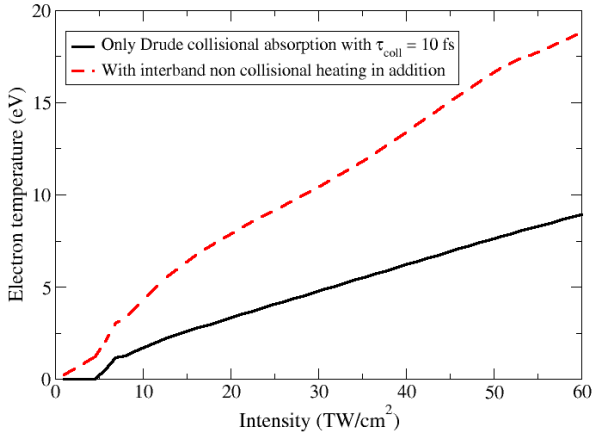

FIG. 5. Evolution of the electron temperature as a function of the maximum laser intensity as estimated with a simplified Drude-like modeling.

We have shown the importance of the non collisional laser heating. For applicative purposes as laser micromachining of materials, a simple expression to evaluate the laser energy deposition is desirable. The starting point is the interband rate for an electron, $w_{1f}(n)$ bridging the bottom sub-band 1 and the final sub-band f, as derived in [13]:

$$w_{1f} = \frac{m}{4\pi\hbar^2 |p_f|} V_{1f}^2 I J_n'^2(B_{1f}) \left[\left(\frac{\pi}{a}\right)^2 - k_n^2 \right] \qquad (2)$$

where n is the number of photons required to bridge resonantly sub-bands 1 to f at wavevector k_n. J_n' is the derivative of the Bessel function with argument $B_{1f} = \frac{1}{\hbar\omega} \frac{e\vec{F}(t).(\vec{p}_f - \vec{p}_1)}{m\omega}$, $\vec{p}_i$ being momenta related to the reciprocal-lattice vector. V_{1f} is the dipolar matrix element. More details on notations and values of parameters relative to this interband rate can be found in [13].

The energy rate is obtained by multiplying Eq. (2) by $\hbar\omega$ and summing over all allowed multiphoton orders. It then has to be weighted by $\Delta k/(\pi/a) = 2ma^2 h\nu_c/\pi^2\hbar^2$ that is the relative part of the Brillouin zone participat-

ing to interband transition due to the collisional broadening (see Fig. 2). Finally, the energy density absorbed per unit of time through the interband process, dU_{nc}/dt, reads:

$$\frac{dU_{nc}}{dt} = \frac{ma\omega n_e(t)\Delta k}{4\pi^2\hbar\,|p_f|} V_{1f}^2 I \sum_n n J_n'^2(B_{1f}) \left[\left(\frac{\pi}{a}\right)^2 - k_n^2\right] \tag{3}$$

where $n_e(t)$ is the electron density in the conduction band. In order to check the reliability of the expression (3) against kinetic calculations and compare its contribution relative to standard collisional absorption, an evaluation of the electron temperature is performed. The conduction electron density is evaluated by solving multiple rate equations [12]. By setting the Drude averaged collision time to $\nu_c^{-1} = 10$ fs accounting mainly for electron-phonon collisions, the evolutions of the electron temperature ($= U/C_e$ with C_e the classical heat capacity) as a function of the intensity including or not the non collisional laser heating are obtained (see Fig. 5). They exhibit similar trends as those provided by solving the quantum Boltzmann equation [13], and values consistent with the present electron energies (because $T_e \simeq E_{max}/2$ [13]). This demonstrates the reliability of this simplified model (2) describing the additional contribution of non collisional heating to the Drude description.

V. CONCLUSION

Photo-emission experiments have been carried out with large band gap dielectric crystals irradiated by near infrared laser femtosecond pulses with intensities below the ablation threshold. The electron energy spectra exhibit a long tail up to energies close to 40 eV for the highest intensities. The underlying electron dynamics has been analyzed through a state-of-the-art modeling based on the Boltzmann kinetic equation including the main excitation/relaxation processes, and the laser driven field acceleration of ejected electrons. Experimental and theoretical energy distributions are in a very good agreement for all considered laser intensities, whereas up to now only the maximum energy of ejected electrons was considered. This direct comparison of the theoretical predictions to the whole experimental electron energy distributions shows that both heating in the bulk and electric field acceleration in the vacuum make comparable contributions to the electron energy gain. The noncollisional direct multiphoton transitions between sub-bands of the conduction band is a major mechanism for electron heating in the bulk of dielectric materials which must be included for the evaluation of the energy deposition. For application purpose as laser micromachining of materials, a simple expression to evaluate the energy deposition by non collisional absorption has been provided.

ACKNOWLEDGMENTS

This project has received funding from the European Union's Horizon 2020 research and innovation programme under grant agreement No 654148 Laserlab-Europe. Henri Bachau is acknowledged for fruitful discussions on high-order harmonics generation in solids.

[1] B. Rethfeld, A. Kaiser, M. Vicanek, and G. Simon, Phys. Rev. B **65**, 214303(1) (2002).
[2] B. Scharf, V. Perebeinos, J. Fabian, and P. Avouris, Phys. Rev. B **87**, 035414(1) (2013).
[3] P. E. Selbmann, M. Gulia, F. Rossi, and E. Molinar, Phys. Rev. B **54**, 4660 (1996).
[4] A. Kaiser, B. Rethefeld, M. Vicanek, and G. Simon, Phys. Rev. B **61**, 11437 (2000).
[5] N. S. Shcheblanov and T. E. Itina, Appl. Phys. A **110**, 579 (2013).
[6] E. N. Glezer, M. Milosavljevic, L. Huang, R. J. Finlay, T.-H. Her, J. P. Callan, and E. Mazur, Opt. Lett. **21**, 2023 (1996).
[7] E.G. Gamaly, Physics Reports **508**, 91 (2011).
[8] Andrius Marcinkevičius, Saulius Juodkazis, Mitsuru Watanabe, Masafumi Miwa, Shigeki Matsuo, Hiroaki Misawa, and Junji Nishii, Opt. Lett. **26**, 277 (2001).
[9] Rafael R. Gattass and Eric Mazur, Nature Photonics **2**, 219–225 (2008).
[10] J. Zhang, M. Gecevicius, M. Beresna, and P. G. Kazansky, Phys. Rev. Lett. **112**, 033901 (2014).
[11] Ralf Menzel, *Photonics: Linear and Nonlinear Interactions of Laser Light and Matter* (Springer, 2001).
[12] B. Rethfeld, Phys. Rev. Lett. **92**, 187401 (2004).
[13] L. Barilleau, G. Duchateau, B. Chimier, G. Geoffroy, and V. Tikhonchuk, Journal of Physics D: Applied Physics **49**, 485103 (2016).
[14] P. Dombi, A. Horland, P. Racz, I. Marton, A. Trugler, J. R. Krenn, and U. Hohenester, Nano Lett. **13**, 674 (2013).
[15] B. N. Yatsenko, H. Bachau, A. Belsky, J. Gaudin, G. Geoffroy, S. Guizard, P. Martin, G. Petite, A. Philippov, and A. N. Vasil'ev, Phys. Status. Solidi. C **2**, 240 (2005).
[16] H. Bachau, A. N. Belsky, I. B. Bogatyrev, J. Gaudin, G. Geoffroy, S. Guizard, P. Martin, Yu. V. Popov, A. N. Vasil'ev, and B. N. Yatsenko, Appl. Phys. A **98**, 679 (2009).
[17] A. Belsky, H. Bachau, J. Gaudin, G. Geoffroy, S. Guizard, P. Martin, G. Petite, A. Philippov, A. N. Vasil'ev, and B. N. Yatsenko, Appl. Phys. B **78**, 989 (2004).
[18] A. Belsky, P. Martin, H. Bachau, A. N. Vasil'ev, B. N. Yatsenko, S. Guizard, G. Geoffroy, and G. Petite, Europhys. Lett. **67**, 301 (2004).
[19] G. Vampa, C.R. Mcdonald, G. Orlando, D.D. Klug, P.B. Corkum, and T. Brabec, Phys. Rev. Lett. **113**, 073901 (2014).

[20] Georges Ndabashimiye, Shambhu Ghimire, Mengxi Wu, Dana A. Browne, Kenneth J. Schafer, Mette B. Gaarde, and David A. Reis, Nature **534**, 521 (2016).
[21] D. Golde, T. Meier, and S. W. Koch, Phys. Rev. B **77**, 075330 (2008).
[22] Mengxi Wu, Shambhu Ghimire, David A. Reis, Kenneth J. Schafer, and Mette B. Gaarde, Phys. Rev. A **91**, 043839 (2015).
[23] Peter G. Hawkins, Misha Yu. Ivanov, and Vladislav S. Yakovlev, Phys. Rev. A **91**, 013405 (2015).
[24] A. Bourgeade and G. Duchateau, Phys. Rev. E **85**, 056403 (2012).
[25] Jacob B. Khurgin, J. Opt. Soc. Am. B **33**, C1 (2016).
[26] P. Mulser, S. M. Weng, and Tatyana Liseykina, Phys. Plasmas **19**, 043301 (2012).
[27] V. Bagnoud and F. Salin, Appl. Phys. B **70**, S165 (2000).
[28] D. Du, X. Liu, G. Korn, J. Squier, and G. Mourou, Appl. Phys. Lett. **64**, 3071 (1994).
[29] Ph. Daguzan, P. Martin, S. Guizard, and G. Petite, Phys. Rev. B **52**, 17099 (1995).
[30] L. V. Keldysh, Sov. Phys. JETP **20**, 1307 (1965).
[31] P. Martin, S. Guizard, Ph. Daguzan, and G. Petite, Phys. Rev. B **55**, 5799 (1997).
[32] A. Belsky, A. N. Vasil'ev, B. N. Yatsenko, H. Bachau, P. Martin, G. Geoffroy, and S. Guizard, J. Phys. IV **108**, 113 (2003).
[33] V. S. Kortov and S. V. Zvonarev, Journal of Surface Investigation. X-ray, Synchrotron and Neutron Techniques **5**, 764 (2011).
[34] K. Ohya, K. Inai, H. Kuwada, T. Hayashi, and M. Saito, Surface and Coatings Technology **202**, 5310 (2008).
[35] C. Mariani, Conf. Proc. Italian Phys. Soc. **82**, 211 (2003).